Soft Matter

PAPER

View Article Online
View Journal | View Issue

Cite this: *Soft Matter*, 2023, **19**, 7202

Homogeneity of liquid metal polymer composites: impact on mechanical, electrical, and sensing behavior†

Anh Hoang,[a] Omar Faruqe,[b] Elizabeth Bury,[a] Chanyeop Park[b] and Amanda Koh *[a]

Received 24th July 2023,
Accepted 10th September 2023

DOI: 10.1039/d3sm00971h

rsc.li/soft-matter-journal

Liquid metal polymer composites (LMPCs) are formed by dispersing eutectic gallium–indium–tin (galinstan) droplets within a soft polymer matrix, such as polydimethylsiloxane (PDMS), resulting in an insulating composite that is suitable for dielectric applications, including wearable sensors and actuators. LMPCs offer a unique combination of robust mechanical performance and desirable electrical properties. While much research has focused on the effects of rigid fillers in polymer composites, the behavior of liquid metal fillers, particularly the impact of homogeneity, has received limited attention. The density disparity between galinstan and the polymer matrix (6.44 g cm^{-3} compared to 0.97 g cm^{-3}) results in the settling of galinstan droplets before curing, especially in matrices with low viscosity, leading to an inhomogeneous composition that may affect material performance. To address this, an innovative approach was introduced that enabled a spatially uniform (homogeneous) dispersion of galinstan droplets in PDMS while preserving the non-conductive nature of the composites. Work described herein evaluates the influence of homogeneity on electrical and mechanical properties as well as performance of LMPCs as pressure sensors. It was found that homogeneity has minimal effect on permittivity and dielectric loss but exhibits a complex behavior with respect to other parameters, including dielectric strength, which is often exacerbated at higher concentrations (≥50 vol%). These findings provide valuable insight that contributes to improved control over the material properties of LMPCs and expands their potential applications in soft robotics and stretchable electronics.

1. Introduction

Stretchable electronics have emerged as a promising field that combines deformable mechanical behavior with high-performance electrical material to overcome the limitations of rigid, bulky, and power-intensive electronics. Traditional rigid electronics are unable to meet the growing demands for flexibility, comfort, and seamless integration with human bodies and the environment. Thus, the development of stretchable electronics necessitates the use of materials that possess both conformability and electrical conductivity, which makes them better suited for applications, such as wearable sensors,[1–3] energy storage,[4,5] electrodes,[6] and actuators.[7]

There are various methods to manufacture stretchable electronics, with one of the most prevalent being the utilization of soft and stretchable elastomers, such as polydimethylsiloxane (PDMS).[8–10] Within this context, PDMS is preferred for making stretchable electronics due to its excellent flexibility and stretchability, thus allowing it to withstand significant deformations exceeding 200%.[11] The mechanical stability of PDMS ensures that the elastomer can maintain its structural integrity even under repeated stretching or deformation.[12] Additionally, PDMS demonstrates remarkable resistance to biodegradation, along with its outstanding biocompatibility and chemical stability.[13–15] These attributes position PDMS as an exceptional material for applications involving biological tissues.[16–18] However, elastomers, including PDMS, generally exhibit poor electrical properties that fall short of the performance requirements for soft electronics.[8,9,19,20]

To address the challenge of subpar electrical behavior in elastomers and create elastic materials with comparable electrical properties to traditional electronics, efforts have been made to enhance their performance. Traditionally, conventional rigid materials such as iron,[21] nickel,[22] and lead[23] have been utilized as fillers to improve electrical behavior of deformable electronic materials. These solid fillers, however, are rigid,

[a] *Chemical and Biological Engineering Department, University of Alabama, 3043 H. M. Comer, Tuscaloosa, AL 35487, USA. E-mail: askoh@eng.ua.edu*
[b] *Department of Electrical Engineering, University of Wisconsin-Milwaukee, Milwaukee, WI, USA*

† Electronic supplementary information (ESI) available. See DOI: https://doi.org/10.1039/d3sm00971h

brittle, and inflexible,[24,25] thus making them unsuitable for the development of human-interfacing devices. Rigid-filled materials are prone to cracking easily and poorly conform to the contours of the human body. In order to facilitate the development of devices that can safely and comfortably interact with the human body while maintaining optimal performance under conditions of curving or stretching, there is a demand for novel materials that can undergo deformation while retaining their electrical properties.

Gallium-based room temperature liquid metals, specifically gallium–indium–tin (galinstan), exhibit a range of interesting characteristics that make them highly appealing for not only stretchable electronics but also diverse fields of application.[26–30] Galinstan has high thermal and electrical conductivity, low toxicity, and essentially no vapor pressure.[31–33] While many applications have utilized liquid metal as a bulk material, such as in printed traces[34–36] or microfluidic channels,[37–39] significant attention has also been directed towards liquid metal polymer composites (LMPCs) as dielectric materials. By dispersing galinstan droplets in a soft polymer matrix such as PDMS, LMPCs demonstrate tunable mechanical and electrical properties. Gallium alloy-based LMPCs exhibit high relative permittivity and low modulus, therefore making them highly suitable for use as deformable dielectric materials in sensors, wearable devices, and actuators.[25,31,33,40]

Despite the abundance of literature on the effects of rigid fillers in polymers, greater understanding is needed with regards to the fundamental behaviors of liquid metal fillers, especially with respect to composite homogeneity. Due to the greater density of galinstan as compared to the polymer matrix (6.44 g cm^{-3} compared to 0.97 g cm^{-3} in this work), galinstan droplets tend to settle before curing, particularly in low viscosity matrices. This results in a spatially non-homogeneous distribution that potentially affects the composite material behavior. Xue *et al.*[41] attempted to make homogeneous LMPCs by jamming the composites with elastic polydimethylsiloxane particles (PPs), however this work resulted in conductive rather than insulating dielectric materials above a critical threshold and did not study LMPCs with high filler volume fractions (>50 vol%). Previous work by Koh *et al.* showed promising behavior of galinstan composites up to 80 vol%,[40] but homogeneity was assumed rather than specifically investigated. As a result, a method is needed that can achieve high galinstan loading, high permittivity, and homogeneity, while maintaining insulating dielectric behavior.

In this work the effect of homogeneity on the properties of LMPCs and their potential as soft dielectric materials is investigated and discussed utilizing a wide range of filler concentrations (5, 10, 25, 50, and 80 vol%). The impact of homogeneity on compressive modulus, permittivity, dielectric loss, breakdown strength, and the resulting pressure sensing capabilities of LMPCs will be presented. Homogenous and inhomogeneous dispersions were analyzed by developing a novel rotating system as a means of fabricating homogeneous LMPCs and overcoming the inherent density mismatch between galinstan and the elastomer. As settling is such a pervasive phenomena for LMPCs, these findings will enable more robust control over material properties and inform future fabrication methods in order to advance the state of the art in soft robotics, stretchable electronics, and pressure sensing devices.

2. Methodology

2.1. Materials

Components to make galinstan were purchased from RotoMetals (San Leandro, CA). Galinstan was prepared by heating and blending 68.5% Ga, 21.5% In, and 10% Sn (by weight) to form a homogenous liquid alloy. Polydimethylsiloxane (PDMS) was purchased from Gelest, Inc. (Morrisville, PA). Molecular weights of vinyl-terminated PDMS and trimethyl-terminated PDMS were 62 700 g mol^{-1} (DMS-V41, 1×10^4 cSt) and 1250 g mol^{-1} (DMS-T11, 10 cSt), respectively. Platinum-cyclovinylmethylsiloxane complex catalyst (800 ppm) and tetrakis(dimethylsiloxy)silane cross-linker, also purchased from Gelest, Inc., were used as curing agents.

2.2. Making composites

LMPCs were formed using a 1 : 3 vol/vol blend of vinyl-terminated (V41) and trimethyl-terminated (T11) PDMS. The composites were prepared at 5, 10, 25, 50, or 80 vol% of galinstan. A Caframo High Torque Overhead Stirrer operating at 1800 rpm for 15 minutes was used for all composite preparations. The mixing time of 15 minutes was selected to achieve a droplet size of 36 ± 8.5 μm for inhomogeneous and 39 ± 7.3 μm for homogeneous LMPCs. Following the mixing step, the catalyst and crosslinker were added and thoroughly mixed for one minute to achieve uniform distribution. Subsequently, the resulting composite was poured into polytetrafluoroethylene (PTFE) molds and cured at 82 °C for 72 hours. To ensure consistent droplet sizes and control the overall droplet concentrations, each LMPC dispersion was diluted to the desired galinstan concentration with additional PDMS from the formulation with the highest loading of 80 vol% galinstan. By adjusting the PDMS content through dilution, the dispersion was effectively standardized. This ensures consistent droplet sizes across all samples and minimizing any potential variations in droplet size as a contributing factor to the observed results. Droplet analysis of all LMPCs is shown in Fig. S1 (ESI†).

Instead of allowing the dispersions to sit at room temperature to induce settling, LMPCs were subjected to an 82 °C curing process immediately after being poured into molds. This approach aims to replicate realistic fabrication procedures, as the settling of liquid metal droplets is often overlooked or not fully understood by researchers. Due to the density differences between galinstan and PDMS (6.44 g cm^{-3} *versus* 0.97 g cm^{-3}), galinstan tends to settle to the bottom of the mold during curing. This results in a LM rich region (bottom) and PDMS rich region (top). Cured samples in which the LM layer was positioned at the bottom and the polymer layer at the top are denoted as "bottom settled". Conversely, when the cured

sample was flipped, resulting in the LM layer at the top and the polymer layer at the bottom, it is referred to as ''top settled''. These terms will be used throughout the manuscript when discussing the characterization of inhomogeneous LMPCs.

To form homogeneous LMPCs, a VWR® Tube Rotator Unit was utilized (image of setup seen in Fig. S2, ESI†). After pouring the mixture into molds, a thin sheet of PTFE was placed on top as a lid and sealed using tightly wrapped aluminum foil. The wrapped assembly was then securely attached to the rotator unit. The rotator provided continuous end-over-end rotation at 18 rpm. The samples were rotated until gelation, defined by the time at which $\tan \delta_r = 1$ (30–45 min, measured *via* rheology shown in Fig. S3, ESI†), within the controlled environment of an 82 °C oven. No settling was observed after this point. Subsequently, the molds were placed flat to cure for the remaining duration of the 72 hours curing time.

To confirm homogeneity, the morphology of cured LMPCs was examined using a Keyence (Itasca, IL) digital microscope (VHX-7000 series). The examination involved analyzing both the cross-sectional and top-down surface views of the samples at multiple points. The average diameter of LM droplets in LMPCs was determined using ImageJ software.

2.3. LMPC electrical characterization

The relative permittivity and dielectric loss of cured LMPCs were examined using a Keysight (Santa Rosa, CA) E4990A Impedance Analyzer with the 16451B Dielectric Test Fixture at frequencies of 500 Hz to 5 MHz. For inhomogeneous LMPCs, permittivity and dielectric loss was measured on both bottom settled and top settled configurations. Both configurations yielded nearly identical results, thus indicating comparable properties; the results discussed herein focus on the bottom settled configuration. Data describing the top settled configuration can be found in the ESI† (Fig. S4).

AC dielectric strength and partial discharge (PD) measurements were performed using a testbed shown in Fig. S5 (ESI†). The testbed was comprised of a high-voltage electrode and a sample container. To prevent surface flashover, each LMPC sample was placed in a container filled with transformer oil. The bottom of the container was built with a thin aluminum plate which allowed the sample to form an electrical connection with the ground plate. A corona sphere was placed on the top of the high-voltage electrode to prevent corona discharge. To monitor the PD activities, a coupling capacitor was connected in parallel to the testbed, and the output of the capacitor was connected to an Omicron MPD 600 PD measurement system. Each LMPC sample was placed inside the testbed, and a 60 Hz sinusoidal voltage was applied. The voltage across the sample was increased steadily until PD signals were detected. The lowest voltage level at which PD starts to occur is called the partial discharge inception voltage (PDIV). The PDIV of each LMPC was recorded and divided by the thickness of the sample to obtain the partial discharge inception electric field (PDIE).

To measure the dielectric strength, the voltage of the high-voltage electrode was gradually increased as the voltage ran across the LMPC sample. The voltage was monitored through a Tektronix MSO44 oscilloscope until the voltage dropped to zero, thus indicating a breakdown of the sample. The breakdown voltage measured was subsequently divided by the thickness of each LMPC to derive the breakdown electric field (E_{bd}). As described previously, both homogeneous and inhomogeneous (settled) LMPCs were investigated. The inhomogeneous LMPCs are divided into two subcategories (*i.e.*, top and bottom settled) depending on whether the liquid metal (LM) rich side is facing the high voltage (HV) electrode or the ground electrode. Specifically, (i) top settled LMPC refers to the case where the HV electrode faced the liquid metal (LM) rich side, (ii) bottom settled LMPC refers to the case where the HV electrode faced the PDMS rich side.

2.3. Mechanical characterization

The compressive modulus of cured LMPCs was evaluated using an Instron (Norwood, MA) Universal Mechanical Testing (UMT) apparatus equipped with a 50 kN load cell and 2-inch diameter steel pressure platens. A controlled compression rate of 5 mm min^{-1} was applied during the testing process. All samples had a diameter of 2 inches and a thickness of 2.5 mm. For inhomogeneous LMPCs, compressive modulus was conducted on both bottom settled and top settled configurations. Both configurations yielded similar results, indicating comparable mechanical properties; the results discussed herein focus on the bottom settled configuration. Data of the top settled configuration can be found in the ESI† (Fig. S6). The initial linear portion of the data was used to determine the compressive modulus.

2.4. Pressure sensing

The pressure sensing performance of cured LMPCs was assessed using samples that shared the same configuration as described in the compression setup section mentioned previously. Concurrently with the Instron apparatus, the composites underwent continuous electrical interrogation using the Keysight Impedance Analyzer at frequencies from 1 to 100 kHz. To measure the effect of compression on capacitance, two thin copper plates, utilized as parallel electrodes, were integrated within the compressive modulus setup and placed on either side of the LMPCs. This electrode configuration allowed for precise monitoring of the composites' electrical response during compressive deformation, as demonstrated in prior work by Bury.[42] These measurements were conducted at a rate of approximately five scans per second to ensure comprehensive data acquisition. A custom MATLAB script was developed to automate the control of electrical measurements and facilitate efficient data processing. Samples were measured in the top and bottom settled configuration.

3. Results and discussion

3.1. Microscopy analysis of LMPC homogeneity

Galinstan is approximately seven times denser than PDMS and as such tends to settle in polymer composites. At room

temperature, LM droplets in prepared LMPCs settled due to gravity leading to the formation of a LM rich region at the bottom and a LM-poor region (*i.e.*, PDMS rich region) at the top, which is the ''bottom settled'' configuration. Inverting, or flipping over, the ''bottom settled'' LMPC configuration resulted in the formation of the ''top settled'' configuration with the LM rich region at the top and the PDMS rich region at the bottom. In this work, both bottom and top settled configurations of inhomogeneous LMPCs were examined. This analysis allows for a more complete assessment of the material's behavior under different physical orientations of LMPCs, therefore providing insights into how the distribution of the liquid metal phase within the polymer matrix affects its properties.

Settling of galinstan began immediately after casting the mixture into the mold and continued over time. While settling may initiate instantaneously, it is important to note that it does not immediately result in a fully settled state, particularly for higher concentrations such as 80 vol%. The work presented here introduces a novel approach to achieve a uniformly distributed composite by developing a rotating apparatus. The method for preparing homogeneous LMPCs involved the utilization of a VWR® Tube Rotator Unit, which facilitated end-over-end continuous rotation during gelation (shown in Fig. S2, ESI†). This rotational motion prevented settling and ensured a uniform distribution of droplets throughout the composite. By continuously rotating the sample, the gravitational force vector acted upon the galinstan droplets in different directions with respect to the mold and overall composite (rather than simply acting to pull droplets to the bottom of the mold), thereby maintaining the homogeneous dispersion of the galinstan within the polymer matrix. This approach resulted in the formation of a homogeneous composite with evenly distributed droplets throughout the material. This method requires no additional fillers, fabrication steps, or interfacial interactions other than that between liquid metal droplets and the curing PDMS pre-polymer.

Digital microscopy images of inhomogeneous (bottom settled) and homogeneous LMPCs at loadings of 5, 10, 25, 50, and 80 vol% are shown in Fig. 1. The cross-sectional images clearly demonstrate the presence of LM settling in the inhomogeneous samples, where galinstan was concentrated at the bottom of the molds. Despite the occurrence of settling, there was a layer of PDMS entirely encapsulating all LM droplets within the composite, and all LMPCs were removed from the mold without any loss of the liquid metal filler. At lower LM loadings (5, 10, and 25 vol%), distinct separation between galinstan and polymer was observed, whereas at higher loadings (50 and 80 vol%), these layers appeared more similar in appearance. With higher LM loading volumes, the viscosities of the LMPCs will tend to increase.[40] The elevated viscosity promoted a more uniform particle dispersion and a more densely packed environment, thus restricting significant separation resulting in a more homogeneous appearance. This agrees with previous studies that have demonstrated that increasing the viscosity of the composite, as indicated by the scaling analysis of the Stokes formula, effectively suppresses the settling of LM particles.[34,41] In contrast, the homogeneous LMPCs fabricated using the rotator setup exhibits a uniform dispersion of galinstan throughout the PDMS matrix at all droplet concentrations.

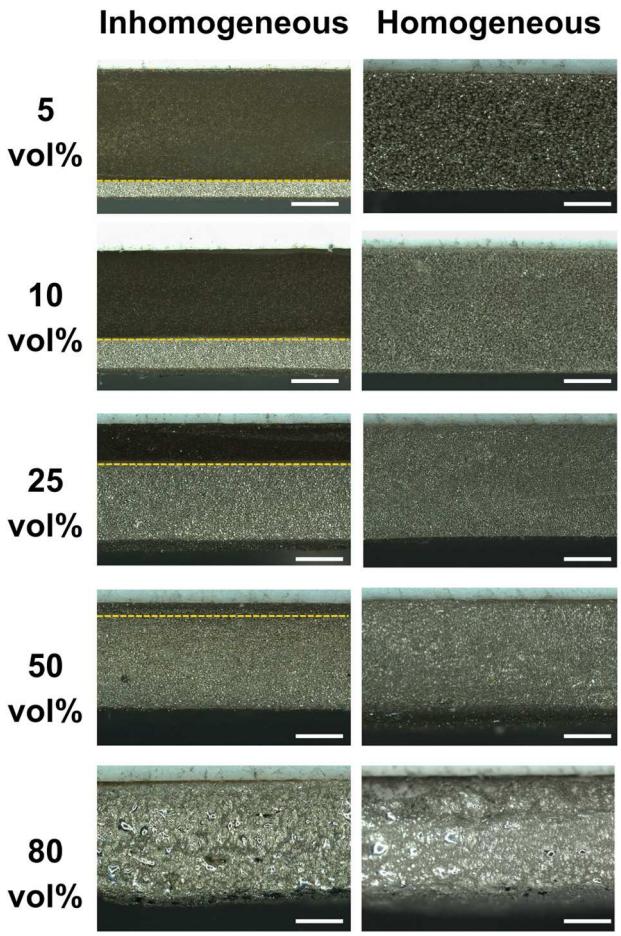

Fig. 1 Digital microscopy images of the inhomogeneous and homogeneous LMPC at 5–80 vol% galinstan. Inhomogeneous LMPCs displaying a bottom settled configuration, characterized by an average diameter of 36 ± 8.5 μm. Homogeneous LMPCs exhibiting a uniform distribution, with an average diameter of 39 ± 7.3 μm. Dotted yellow line indicates the border between the LM rich (below the line) and PDMS rich (above the line) regions. Scale bar is 1 mm. Top view and droplet analysis of all LMPCs can be found in Fig. S1 (ESI†).

3.2. LMPC dielectric permittivity and loss

For dielectric materials, it is generally desirable to have high permittivity and low dielectric loss.[43] These characteristics are pivotal in determining the efficacy of polymer composites for dielectric applications such as soft and stretchable electronics.[3,4,6,31,44,45] An increased relative permittivity indicates enhanced dielectric performance *e.g.*, the material's ability to store electrical energy effectively. The relative permittivity and dielectric loss of both inhomogeneous (bottom settled configuration) and homogeneous LMPCs was evaluated at 5, 10, 25, 50, and 80 vol% of galinstan (Fig. 2). Relative permittivity of bottom settled and top settled configurations of the inhomogeneous LMPCs are similar. Therefore, this discussion focuses solely on

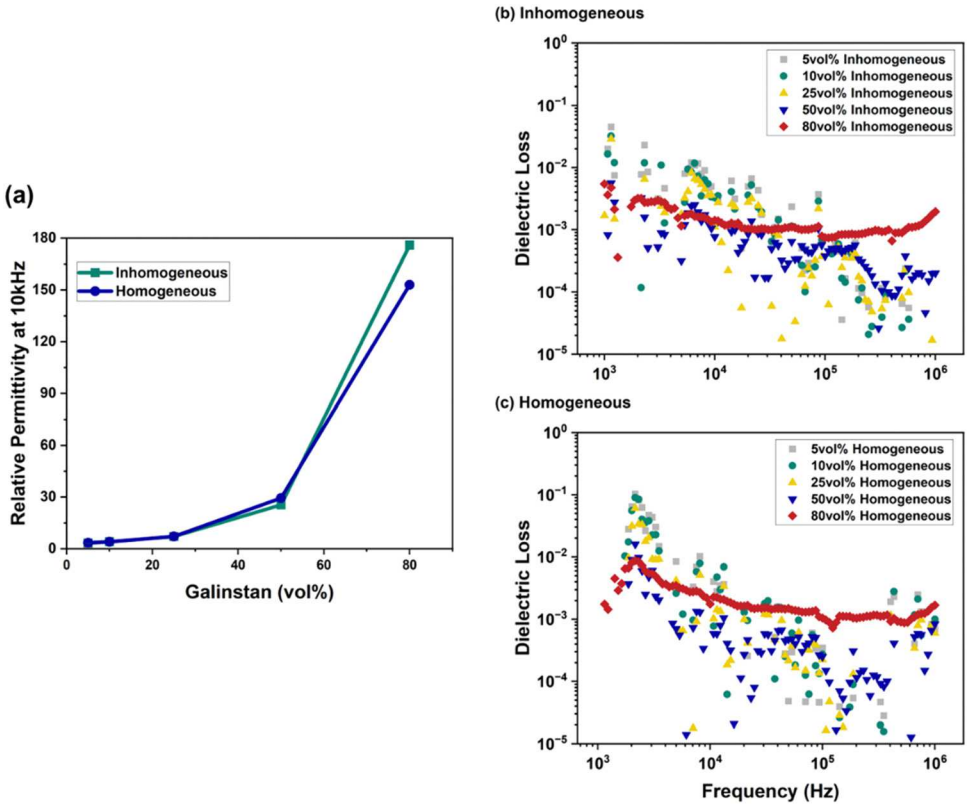

Fig. 2 (a) Relative permittivity of LMPCs at 10 kHz with respect to loading. (b) Dielectric loss of cured inhomogeneous (bottom settled) and (c) homogeneous LMPCs with respect to frequency.

the data obtained from the bottom settled samples. The data for top settled can be find in Fig. S4 (ESI†). Permittivity increased with greater galinstan loading, which is consistent with what has been seen in prior work with liquid metal composites.[40,42,44] The measured permittivity values align with the measurements conducted by Bartlett *et al.*[44] up to 50 vol% and with Koh *et al.*[40] up to 80 vol%. The comparability of the results across the studies by Bartlett and Koh, which used similar droplet sizes ($\sim$30 μm) and the same PDMS formulations, further strengthens the observed similarities in permittivity trends.

Permittivity of dielectric materials is calculated based on a bulk capacitance measurement by the impedance analyzer. Such measurements consider the overall dielectric behavior of the material as a whole, rather than focusing on specific localized regions or interfaces. However, the settled material can theoretically be considered as two dielectric materials in series with two distinct permittivity values using eqn (1) and (2):

$$C = \frac{\varepsilon_r \varepsilon_0 A}{d} \quad (1)$$

$$C_T = \frac{1}{\left(\frac{1}{C_L}\right) + \left(\frac{1}{C_P}\right)} \quad (2)$$

where ε_r is the calculated relative permittivity, ε_0 is the permittivity of free vacuum, A is capacitor area, d is capacitor thickness, C_T is the total measured capacitance, C_L is the capacitance of the LM rich region and C_P is the capacitance of the PDMS rich region. To understand the reason why homogenous and inhomogeneous LMPCs permittivity values are similar, it is important to note that both local permittivity and region thickness impact the overall measured capacitance. C_T can be maximized if C_L and C_P are equivalent, but these values being equivalent is not the same as the permittivity values being equivalent. It is clear from Fig. 1 that the thicknesses of the LM rich and PDMS rich regions are not only unequal but also different for each concentration of liquid metal up to the extreme case of 80 vol% for which the inhomogeneous and homogenous LMPCs appear similar under microscopy. Using eqn (1) and (2), C_T tends towards the capacitance of C_P with increasing contribution of C_L as the local permittivity of the LM rich region increases and the thickness of the PDMS rich decreases. As Fig. 1 shows, the PDMS rich region has some concentration of liquid metal. This results in permittivity (and C_P) greater than that of the neat polymer while the LM rich region has a significantly higher permittivity. The similar permittivities of the homogenous and inhomogeneous LMPCs suggests that the thickness and relative dielectric permittivity values of the two regions of the inhomogeneous LMPCs balance such that the resultant bulk permittivity is similar to that of the homogeneous material. This behavior is seen for both the top settled and bottom settled LMPC samples, further reinforcing the bulk nature of the permittivity value.

Xue *et al.*[41] also examined the effect of homogeneity on dielectric properties of LMPCs although the homogeneity was induced by jamming with jagged PDMS particles rather than the rotation method discussed here. Interestingly, composites made by Xue *et al.* demonstrated a transition from dielectric behavior to conductivity in LMPCs once galinstan concentration exceeded ~36 vol%. The transition to conductive behavior was not seen in this work as the layer of PDMS between galinstan droplets was consistently preserved and no mechanical disturbance of the droplets, either through intentional sintering, interfacial interactions, or material handling, ruptured the LM droplets. Instead, the phase angle of both the inhomogeneous and homogeneous LMPCs in this study remained constant at −90 degrees for both types of LMPCs (Fig. S7, ESI†). A phase angle of −90 degrees indicates that the material is purely capacitive, acting as a dielectric and insulator, with no significant conductivity.[42] This was observed even at high galinstan concentrations (80 vol%), where conductivity may be expected to become more prominent. The adherence to capacitive behavior was consistent for homogeneous, top settled, and bottom settled LMPCs.

Homogeneous LMPCs made using the rotator method employed in this study effectively preserved the non-conductive nature of LMPCs. The gentle rotational motion facilitated a uniform distribution of liquid metal droplets did not alter the fundamental characteristics of the composite structure. The non-conductive behavior of LMPCs arises from the continuous PDMS matrix that surrounds the dispersed liquid metal droplets. The PDMS acts as an insulator and hinders the movement of electric charges within the composite. During the rotation process, the rotational movement facilitates the even dispersion of the liquid metal droplets within the PDMS matrix, thereby preventing settling and achieving homogeneity. The rotation method does not introduce any additional additives or interactions to the composites. The non-conductive behavior is solely attributed to the intrinsic characteristics of the PDMS matrix and the interrupted arrangement of the liquid metal droplets. Therefore, the rotation technique serves as an effective means of achieving homogeneity without compromising the non-conductive nature of LMPCs, thus making it a valuable approach for various applications requiring both uniform dispersion and electrical insulation.

Fig. 2b and c show the dielectric loss for galinstan loading from 5 to 80 vol%. Dielectric loss is associated with the dissipation of electrical energy in a material. For dielectric materials, a low loss value is highly desired. In the context of LMPCs, a low dielectric loss signifies that the material exhibits minimal energy dissipation and is, therefore, a good insulator. Furthermore, it suggests that there are limited pathways for the flow of electrical current resulting in efficient insulation and the ability to retain and store electrical energy.[44] Here, both the inhomogeneous and homogeneous samples exhibit low levels of dielectric loss, which suggests the absence of significant conductive pathways within the settled sample. This observation is consistent with previous work by Calabrese *et al.*, who also saw that increasing galinstan concentration has little effect on the loss value of the composites.[46]

3.3. Breakdown electric field and partial discharge measurement

The breakdown electric fields (E_{bd}) of the LMPCs are presented in Fig. 3. The results indicate that the E_{bd} of the composites decreases with increasing galinstan concentration from 5 to 80 vol% for both homogenous and inhomogeneous LMPCs. A similar declining trend was observed and reported in previous work by Calabrese *et al.* on PDMS-galinstan-barium titanate and PDMS-galinstan-iron composites.[46] As galinstan is highly conductive, the voltage drop through it is negligible, while there is a larger voltage drop (*i.e.*, electric field) through the resistive PDMS region. As a result, as the concentration of highly conductive fillers increases, PDMS experiences greater electric field stresses, and the breakdown voltage of the composite decreases. For filler concentrations up to 50 vol%, the bottom settled LMPC shows higher breakdown strength than the homogeneous and top settled samples. In the settled LMPCs, PDMS rich zones serve as an insulating layer, while the LM rich zones serve as conductive layers. For the bottom settled samples, the HV electrode faces the PDMS rich zone, resulting in higher breakdown strength mainly because the lack of liquid metal near the triple point edges does not cause a significant electric field increase. The homogeneous samples have nearly identical E_{bd} compared to that of the top settled samples for filler concentrations up to 25 vol% because, in both cases, liquid metal fillers exist near the triple point edge and increase electric field. The E_{bd} of the homogenous LMPCs dropped by 95.8% as the filler concentration increased from 25 to 50 vol%. In contrast, the E_{bd} of a 50 vol% top settled LMPC sample dropped only by 14.5% from that of the 25 vol% top settled sample, therefore indicating that liquid metal filler homogeneity affects dielectric strength, which is explained in the following section. All samples display low breakdown strengths at 80 vol% (<100 V mm^{-1}) because the PDMS rich region is largely lost and the LM is mostly homogeneously distributed even for the "settled" LMPCs (Fig. 1). As such, it is

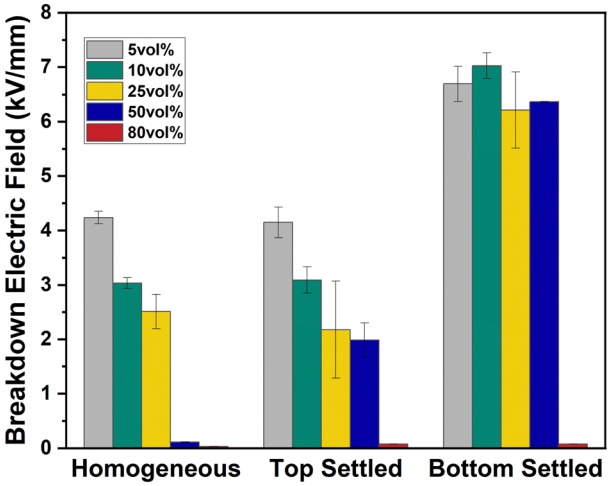

Fig. 3 Breakdown electric field of LMPCs as a function of homogeneity and galinstan concentration.

clear that the difference in dielectric breakdown strength between homogeneous and inhomogeneous composites reduces with increasing filler concentration.

According to the breakdown electric field results shown in Fig. 3, homogenous LMPCs have a much lower E_{bd} at 50 vol% galinstan as compared to the top settled samples. In LMPCs, the LM fillers are insulated by PDMS, and the thickness of the PDMS along the path of LM fillers plays a vital role in breakdown strength as lower insulation thickness translates to higher electrical stress. Fig. 4 shows the conceptual cross-sectional model of homogenous and inhomogeneous LMPCs. Here, the distance d_{PDMS} represents the thickness of neat PDMS from the top to bottom electrode along the path through LM fillers.

Fig. 4 shows a model rectangular homogeneous and inhomogeneous LMPC with width w, thickness h, and n number of spherical LM droplets with a diameter of d. In the case of the homogenous sample shown in Fig. 4a, there are n_1 number of LM droplets across the width w and n_2 number of LM fillers across the thickness h with each LM separated by distance x. The distance x can be calculated by solving the following equations.

$$w = n_1 d + (n_1 - 1)x \quad (3)$$

$$h = n_2 d + (n_2 - 1)x \quad (4)$$

$$n = n_1 - n_2 \quad (5)$$

Then distance x can be used to calculate d_{PDMS}.

$$d_{PDMS} = (n_2 - 1)x \quad (6)$$

However, for inhomogeneous samples, one can neglect inter-filler distance, because LM fillers are densely packed at the top of the samples as illustrated in Fig. 4b. In this case, the following equations can be derived:

$$w = n_1 d \quad (7)$$

$$n_2 = \frac{n}{n_1} \quad (8)$$

$$d_{PDMS} = h - n_2 d \quad (9)$$

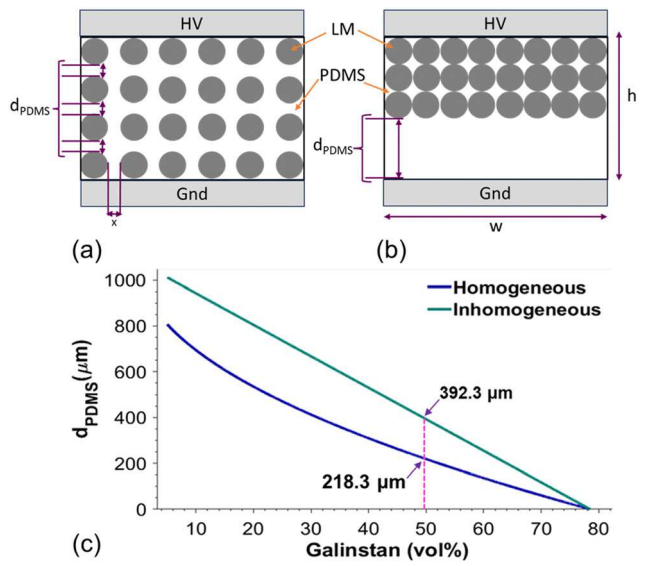

Fig. 4 Conceptual models of (a) homogenous, (b) inhomogeneous samples, and (c) net PDMS thickness (d_{PDMS}) *vs.* galinstan concentration (vol%).

Fig. 4c shows d_{PDMS} *versus* galinstan concentration (vol%) curves of homogenous and inhomogeneous LMPC samples with d = 39 μm, w = 5.4 mm, and h = 1.08 mm. In the case of the homogeneous sample, d_{PDMS} is 218.3 μm at 50% filler concentration, whereas the inhomogeneous sample has a d_{PDMS} of 393.3 μm. The lower d_{PDMS} for the homogenous sample causes higher electric field stress and facilitates the electrons avalanche process that leads to dielectric breakdown at a lower voltage.

It is interesting to note that the homogeneous and inhomogeneous curves appear to converge around 79% galinstan concentration. This indicates that the settling of the LM gradually disappears at such high concentration, and the LM distribution becomes more homogeneous. This phenomenon is also seen in the 80 vol% LMPC microscopy (Fig. 1). Due to the increasing homogeneity with increasing filler concentration, at 80 vol% the inhomogeneous samples exhibit similar breakdown strength as that of the homogenous samples. It should be noted that the distance calculated could be different from the actual inter-filler distances in the fabricated LMPC samples as the LM droplets are assumed to be 2D circles perfectly homogeneously distributed. Despite these simplifications, the findings from the model and the differences in the d_{PDMS} between homogeneous and inhomogeneous LMPC samples provides insight into the experimental results of Fig. 3.

Partial discharges (PD) are electrical discharges that are much smaller in magnitude compared to a full dielectric breakdown. Though subtle, the service life of insulation is significantly reduced as a result of erosion caused by PD, particularly when there are numerous and repetitive PDs under AC voltage stress.[47] As a result, PD is widely used for assessing the insulation quality of dielectric materials.[48] The PD behavior of LMPCs, as seen in Fig. 5, demonstrates that the PDIE of homogeneous and top settled samples decreases with increasing filler concentration. This results from a decrease in the volume of resistive PDMS with increasing galinstan concentration. Due to the high conductivity of galinstan, as its concentration increases, the electric fields increase in the remaining PDMS volume. However, increasing filler concentration had a relatively small impact on the PDIE of the bottom settled samples, up to 25 vol% galinstan. The PDIE values of the bottom settled LMPCs are comparable to those of neat PDMS (Fig. S8, ESI†). This is likely due to the lack of dispersed galinstan near the surface in contact with the HV electrode. However, as the filler concentration increases further to 50 vol%, the PDIE of all three LMPC homogeneity categories decreases steeply. The PDIE of samples with 80% galinstan concentration further decrease below 100 V mm^{-1}, likely due to the diminishing filler settling in the inhomogeneous samples.

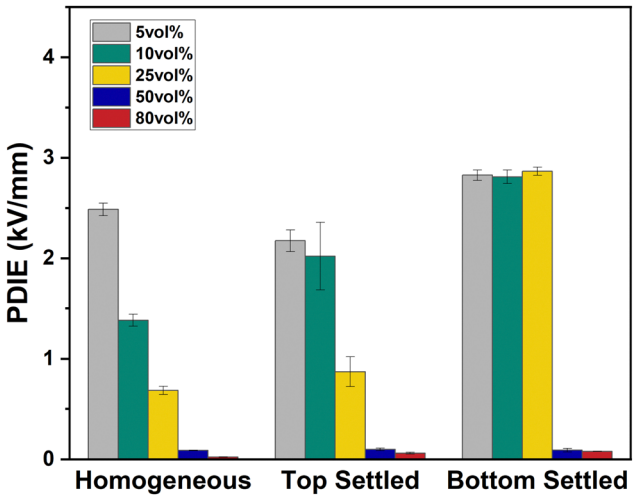

Fig. 5 PDIE of LMPCs as a function of homogeneity and galinstan concentration.

3.4. Electric field finite element analysis

Finite element analysis (FEA) models of each LMPC type were created to better understand the impact of filler distribution on the electric field distribution within the LMPCs. Two-dimensional FEA models representing the cross-sections of the LMPCs were developed. Homogenous, top settled, and bottom settled LMPCs with 5, 10, and 25 vol% filler concentrations were modeled. The electric field distributions of the composites with 25 vol% filler concentration and the neat PDMS are shown in Fig. 6. The fillers are placed randomly in the PDMS in the homogeneous LMPC. In the case of the bottom settled LMPC, the fillers are accumulated on the bottom surface of the sample. To create the top settled LMPC, the bottom settled LMPC model was flipped. The material properties of galinstan (conductivity of 3.46×10^6 S m^{-1} and relative permittivity of 1) were assigned to the circles,[49,50] whereas the properties of PDMS (conductivity of 5.0×10^{-15} S m^{-1} and relative permittivity of 2.86)[51,52] were assigned to the spaces between the fillers. On the top side of the modeled LMPC, a 5 kV 60 Hz sinusoidal voltage was applied, while the bottom side was set to 0 V. From the electric field distribution plots in Fig. 6, one can observe that the maximum electric field occurs in the triple point edge where the three different types of materials (*e.g.*, metal electrode, insulator, and dielectric oil) meet. The figure shows that the maximum electric field at the triple point edge increases as the galinstan concentration increases. According to A. Küchler[53] the maximum electric field at a triple point is proportional to the ratio of the relative permittivity of the solid dielectric (LMPC) and the surrounding medium (oil). In other words, the greater the permittivity difference between the LMPC and oil, the greater the triple-point electric field.

As seen in Fig. 2, the relative permittivity of the LMPCs increases with increasing galinstan concentration. At a given galinstan concentrations, the bottom settled sample has the lowest maximum electric field and followed by homogeneous then top settled samples, as shown in Fig. 3. In the case of homogenous and top settled samples, the electric field increases further as the liquid metal droplets are in close proximity to the triple point. The presence of conductive liquid metal droplets near the triple point forces greater voltage drop to occur in the PDMS around the triple point, thus increasing

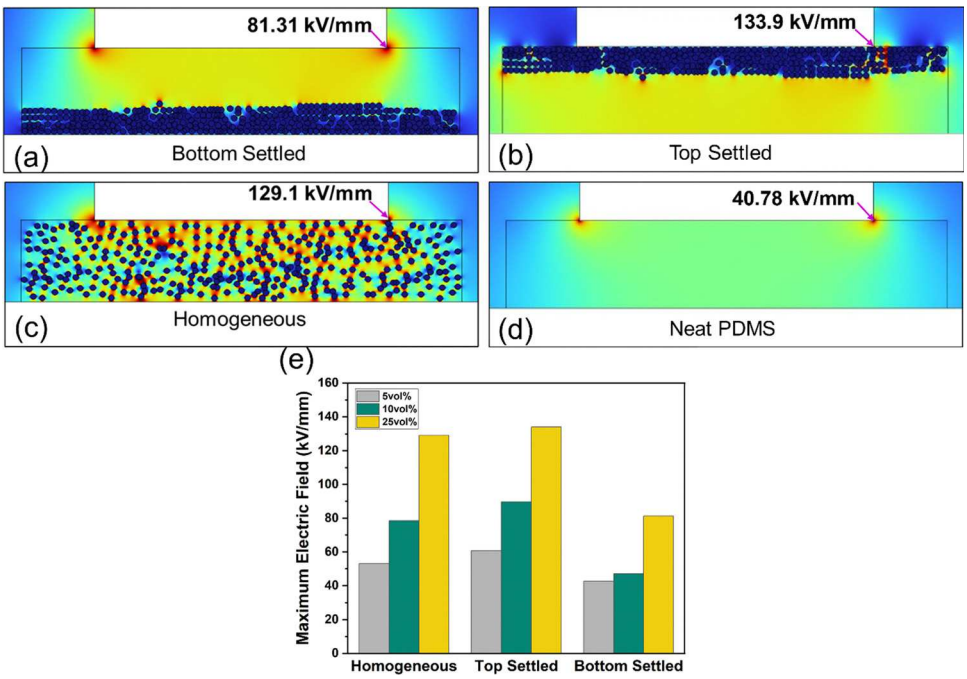

Fig. 6 Electric field distribution of LMPC (a) homogenous, (b) top settled, (c) bottom settled, (d) neat PDMS at 5 kV, and (e) numerically analyzed maximum electric field at 5 kV.

the electric field in the region. Electric breakdown in solid dielectrics is initiated by the field emission of electrons from an electrode.[53] Free electrons injected into a solid gain sufficient energy under high electric fields, cause ionization collisions, and form electron avalanches. Hence, the high electric field generated near the triple point region plays a key role in triggering a breakdown of solid insulating materials.

The non-uniform and high electric fields created near the triple point edge also give rise to the observed PD behavior. Surface discharges, a type of PD on dielectric surfaces, start to occur as the local electric field exceeds the dielectric strength of the surrounding medium.[53] Therefore, LMPCs with a stronger localized electric field simulated under a given voltage are expected to have lower measured PD inception voltages. The trend of the simulation is consistent with the experimental data of up to 25 vol% galinstan. A higher electric field in a dielectric simulated at a given voltage translates to a lower measured E_{bd} and PDIE.[46]

3.5. Compression testing of LMPCs

Compressive modulus is a measure of a material's stiffness or resistance to deformation under a compressive force and a key factor to its use in pressure sensing. Compressive modulus of both inhomogeneous and homogeneous LMPCs, as well as neat PDMS, were evaluated at 5, 10, 25, 50, and 80 vol% of galinstan (Fig. 7). Neat PDMS, represented by the black dotted line, exhibited the highest compressive modulus of 520 kN m^{-2} compared to all LMPCs. Overall, the addition of galinstan resulted in a decrease in the compressive modulus of the polymer composites. The reduction in modulus is expected as replacing relatively high modulus polymer with relatively low modulus fluid should reduce the overall modulus, although the impact of the galinstan oxide shell is non-negligible and oftentimes complex. The compressive modulus data also aligns with common observations reported in the literature, where the incorporation of liquid metal in polymer composites tends to reduce the overall material stiffness.[25,44,46,54] The impact of homogeneity differed based on concentration, although compressive modulus values for 25 vol% and lower were similar. The magnitude of the modulus reduction varied between these loadings. At higher loading concentrations, the effect of homogeneity on the compressive modulus became more pronounced for homogeneous materials. For 50 vol% settled LMPCs, the settled material exhibited a 40% decrease in compressive modulus compared to the neat polymer while the homogenous material showed an 80% decrease in compressive modulus.

A recent study conducted by Hu *et al.*[55] also observed a decrease in modulus when liquid metal was homogeneously dispersed in a PDMS matrix, especially at 50 vol%. In their study, they attributed the decrease in stiffness to Eshelby's classical theory of inclusions, which predicts a reduction in the elastic modulus of composites containing liquid inclusions. However, Eshelby's theory should suggest that as the liquid metal concentration increases there should be a continued decrease in modulus, rather than the largely concentration-independent modulus shown in Fig. 7. The average droplet size of each LMPC as well as size dispersity was roughly equivalent regardless of galinstan concentration due to the method of LMPC fabrication. Therefore, a change in the jamming of smaller and larger droplets is unlikely the cause of the modulus in high concentration LMPCs. Instead, the increase in liquid material in the LMPC, and the resulting reduction in modulus, may be balanced by the introduction of more rigid liquid metal oxide, which would encapsulate every droplet.[31,54] In general, however, softer material that can simultaneously achieve high permittivity is ideal for sensitivity and deformable dielectrics broadly.

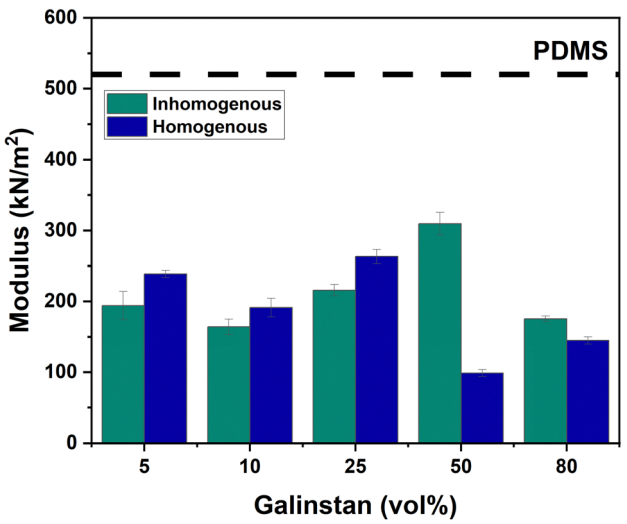

Fig. 7 Compressive modulus of neat PDMS, cured inhomogeneous (bottom settled) and homogeneous LMPCs at various loading vol%.

3.6. Sensitivity and linearity of LMPCs as pressure sensor elements

The development of pressure sensors that exhibit high sensitivity and reliability has received significant attention in research due to a wide range of applications in fields such as healthcare[2,3,31,56] and robotics.[44,45,57] The ability to accurately measure and monitor pressure is crucial for ensuring safety, optimizing performance, and enabling precise control for these applications. In this study, the potential of LMPCs as promising materials for capacitive stress sensors was explored. The unique combination of mechanical and electrical properties exhibited by LMPCs makes them highly suitable for pressure sensing applications. LMPCs can achieve high relative permittivity values, reaching up to 170 (Fig. 2), while maintaining their soft and deformable nature, with a modulus as low as 100 Pa (Fig. 7). The high relative permittivity enables efficient charge storage and responsive behavior to changes in applied electric fields, thereby enhancing the capacitive response of the sensor for precise detection and measurement of small pressure variations. Simultaneously, the low modulus ensures that the sensor can readily deform and conform to applied pressure, possess optimized contact area, and ultimately lead to enhanced sensitivity. To evaluate the pressure sensing performance of LMPCs, pressure sensors were fabricated using a

method similar to that of Bury *et al.*[42] LMPCs were subjected to the same load over repeated measurements, conducted in triplicate, and yielded repeatable stress–strain curves. The composites showed no signs of structural or physical damage throughout the entire experiment.

Pressure (kPa) *versus* capacitance (fF) of both top settled and bottom settled configurations were tested and compared to the homogeneous LMPCs (Fig. 8). The sensitivity of the sensors under compression was determined by the change in capacitance with respect to pressure in the linear regime of stress–strain curve, *i.e.*, the slope of the curves in Fig. 8 with units of (fF kPa^{-1}). This sensitivity is enumerated in Fig. 9a.

The sensitivity of LMPCs was found to increase with higher filler concentration, as expected.[42,58,59] As seen in Fig. 9, homogeneous LMPCs with a filler concentration of 5 vol% exhibited a sensitivity of 169 fF kPa^{-1}, while a tenfold increase in concentration to 50 vol% resulted in a sensitivity of 1255 fF kPa^{-1}. This value continued to increase and reached a sensitivity of 4836 fF kPa^{-1} at 80 vol%. These results consistently correspond to the permittivity measurements presented in Fig. 2, where LMPCs demonstrated higher permittivity with increasing loading. As a result, the enhanced permittivity directly contributes to the improved sensitivity of LMPCs as it enables the composites to exhibit more pronounced electrical responses, even in the presence of subtle pressure changes. This fundamental trend can be seen in both homogeneous and inhomogeneous LMPCs.

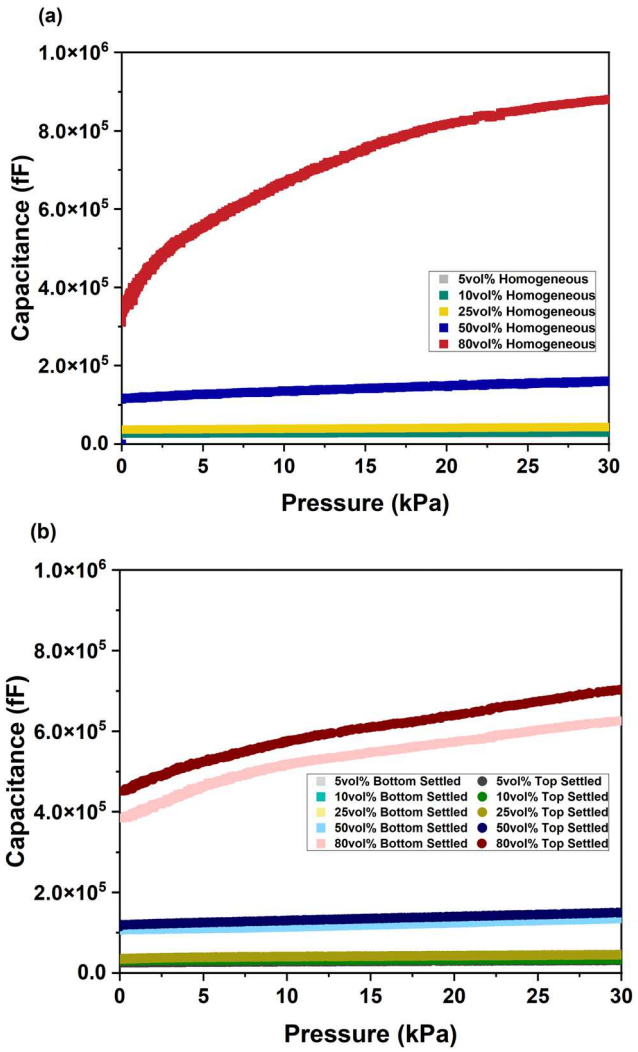

Fig. 8 Capacitive response of (a) homogeneous, (b) bottom settled, and top settled LMPCs under compression at various loading vol%.

Both the bottom and top settled configurations of inhomogeneous LMPCs were examined to evaluate their impact on performance. It was observed that configuration had minimal influence on LMPCs with filler loading below 25 vol% but showed significant effects above this threshold value. For a filler concentration of 5 vol%, the sensitivity of the bottom and top settled configurations was 198 fF kPa^{-1} and 192 fF kPa^{-1}, respectively. At a concentration of 10 vol%, the sensitivity of the bottom and top settled configurations was 140 fF kPa^{-1} and 146 fF kPa^{-1}, respectively. However, as the galinstan concentration increased, the top settled LMPCs demonstrated significantly higher sensitivity than the bottom settled LMPCs. At 50 vol%, the top settled exhibited a sensitivity of 761 fF kPa^{-1}, which was notably higher than the sensitivity of the bottom settled at 657 fF kPa^{-1}. Similarly, at 80 vol% the top settled displayed a sensitivity of 3288 fF kPa^{-1}, which was roughly two times higher compared to the bottom settled at 1526 fF kPa^{-1}. The higher sensitivity observed in the top settled LMPCs configuration can be attributed to the proximity of the liquid metal droplets to the pressure application (*i.e.*, the upper pressure platen). In the top settled configuration, the liquid metal layer is positioned directly under the platen, thereby enabling a direct transmission of pressure to what is the softer region of the composite. This proximity resulted in a more pronounced change in the electrical response of the LMPCs, thus leading to higher sensitivity. In contrast in the bottom settled configuration, the region directly in contact with the application of pressure was PDMS-rich and thus more rigid causing a reduced propagation of the force. This resulted in a less responsive electrical signal.

While the settled configurations (bottom settled and top settled) showed varying sensitivity levels, the homogeneous LMPCs consistently exhibited the highest sensitivity at higher galinstan loadings, specifically above 25 vol%. For a filler concentration of 50 vol%, the sensitivity of the homogeneous LMPCs was measured as 1255 fF kPa^{-1}, which was higher than both the bottom settled (657 fF kPa^{-1}) and top settled (761 fF kPa^{-1}) LMPCs. Similarly, at 80 vol%, the homogeneous LMPCs demonstrated a sensitivity of 4836 fF kPa^{-1}, surpassing the sensitivities of the bottom settled (1526 fF kPa^{-1}) and top settled (3288 fF kPa^{-1}) LMPCs. The impact of homogeneity on the LMPCs mechanical and electronical properties become more apparent at concentrations exceeding 25 vol%.

The behavior of LMPCs as pressure sensors is influenced by the homogeneity and mechanical properties, particularly at different galinstan concentrations. At lower concentrations (<25%), the inhomogeneous behavior dominates the composite's response and leads to slightly higher sensitivities as compared to the homogeneous LMPCs. This is consistent with

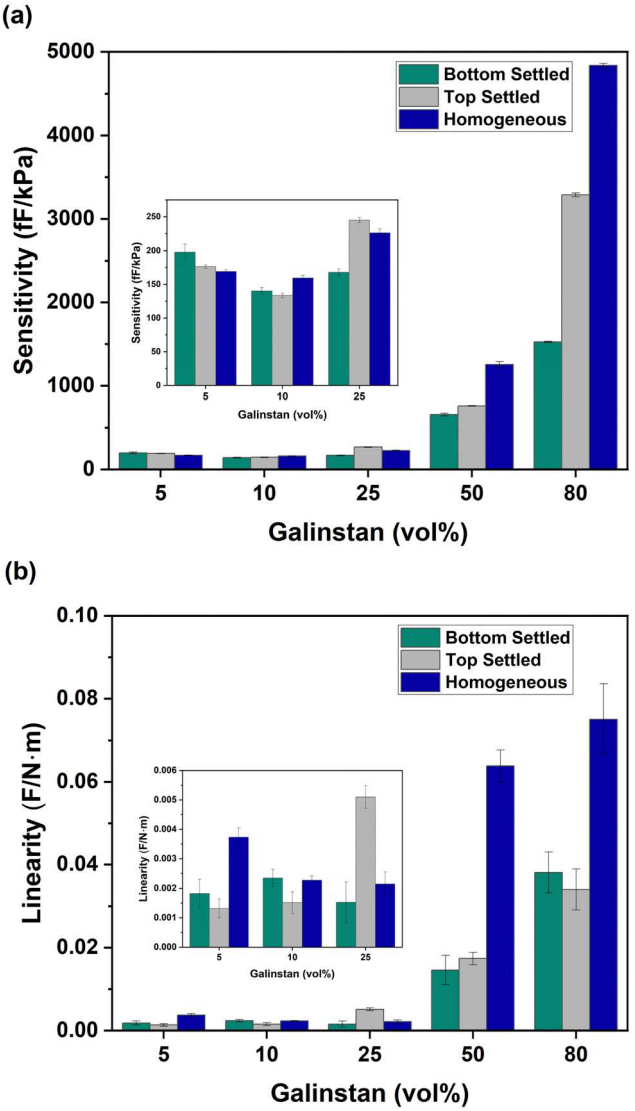

Fig. 9 (a) Sensitivity of homogeneous and inhomogeneous LMPCs. Sensitivity (fF kPa^{-1}) is the slope of the change in capacitance with increasing pressure. (b) Linearity (F N^{-1} m^{-1}), or permittivity dependence on compression, of homogeneous and inhomogeneous LMPCs.

the compressive modulus data, where the inhomogeneous LMPCs exhibit lower modulus values compared to the homogeneous LMPCs. The lower modulus results in a softer material that exhibits greater deformability and sensitivity to pressure variations, thereby contributing to slightly higher sensitivity as pressure sensors. However, beyond 25 vol% galinstan, a threshold is reached, and the dominance shifts to the homogeneous LMPCs. At this point, the homogeneous LMPCs become the primary driver of the overall behavior. This is likely due to a lower modulus which leads to a significant increase in sensitivity, as observed in Fig. 7 and 9. Essentially, modulus is critical to sensitivity both as a bulk material, which is the only mode for homogeneous dispersions, and in terms of local modulus, as would be the case for inhomogeneous dispersions.

Permittivity is used as a measurement of dielectric performance because it is critical to the electrical output as seen from eqn (1). In this equation, only capacitance and thickness are typically treated as variables while area is a device parameter and permittivity is a material constant. However, prior work has demonstrated that treating permittivity as a constant while under load is often inaccurate.[60] To determine how load-independent LMPC dielectric behavior is, permittivity linearity was also measure. If a dielectric material is perfectly load-independent, permittivity linearity should be zero. The higher the permittivity linearity value the more load dependent the material dielectric behavior is.

Despite an order of magnitude increase in the high concentrations of 50 and 80 vol%, the linearity values consistently remain under 0.1 F N^{-1} m^{-1}. These values are roughly 10 times lower than those reported for rigid-filled PDMS composites,[42] therefore suggesting that the permittivity in the LMPCs remains unaffected by compressive forces. This observation supports the notion that the permittivity of the LMPCs used in this study is load independent, which aligns with the findings of Bury *et al.*[42] Their study revealed that rigid fillers, such as iron, impose additional stress on the encapsulating polymer and affect its polarizability. In contrast, galinstan, as a liquid and deformable filler, mitigates the forces exerted on the polymer matrix and leads to reduced interactions between the rigid particles and the polymer. This can be attributed to the application of the Maxwell stress equation, as suggested by Di Lillo *et al.*,[61] which states that the change in electric field within the material is proportional to the change in polarization. This value exhibits a direct proportionality to the relative permittivity, and it remains independent of deformation when a constant electric field is applied.

There is no consistent trend between permittivity linearity and homogeneity up to 25 vol% (Fig. 9b). At 50 and 80 vol%, linearity is significantly higher for homogenous samples than for inhomogeneous samples. While galinstan has less of an effect on matrix polarizability than other rigid fillers, increasing concentration is likely to increase any effect that may be present. When the LM is evenly distributed throughout the LMPC, there is more PDMS in the interstitial spaces between liquid metal droplets as demonstrated in Fig. 4. Consequently, any change in polarization of the PDMS directly adjacent to galinstan droplets would be greater since a greater volume of PDMS would be affected. Nevertheless, even at the greatest linearity value of 0.075 F N^{-1} m^{-1} for homogenous 80 vol% LMPC, the permittivity is significantly more load-independent than comparable rigid-filled composites and thus will result in a simpler pressure sensor.

4. Conclusions

Galinstan concentration as well as homogeneity have a significant impact on the electrical and mechanical properties of LMPCs. Increasing the galinstan concentration leads to higher permittivity while the influence of homogeneity on permittivity

and dielectric loss is minimal, thus indicating that relative permittivity primarily represents a bulk measurement. The same was not seen for dielectric strength for which the orientation of LMPC matters significantly. For dielectric strength, a concentration threshold of 25 vol% has been identified beyond which the breakdown strength experiences significant decreases. This threshold also affects the mechanical properties of the LMPCs. Below the identified threshold, inhomogeneous behavior leads to decreased modulus, while beyond the threshold, homogeneous LMPCs were characterized by low modulus and high sensitivity. This relationship highlights the critical role of modulus in determining the sensitivity of LMPCs, whether as a bulk material in the case of homogeneous dispersions or in terms of local modulus for inhomogeneous dispersions. For pressure sensing, higher loading of liquid metal fillers consistently corresponds to higher permittivity and increased sensitivity while the impact on rigidity is less straightforward. Therefore, the modulus is essential for determining the overall sensitivity of LMPCs, regardless of their homogeneous or inhomogeneous nature.

Using the method developed herein, the homogeneity of LMPCs can be controlled. Which enables tunability of electrical and mechanical properties, and thus sensitivity under load. Whether the material is used for robotics, wearable devices, prosthetics, or other applications, the identification of a galinstan concentration thresholds with respect to dielectric strength and the importance of modulus in sensitivity offer valuable insights for the design and optimization of LMPCs.

Author contributions

A. H.: data curation, formal analysis, investigation, methodology, visualization, writing – original draft, writing – review and editing; O. F.: data curation, formal analysis, investigation, methodology, visualization, writing – original draft, writing – review and editing; E. B.: data curation, investigation, methodology, writing – review and editing; C. P.: conceptualization, funding acquisition, project administration, resources, supervision, methodology, writing – original draft, writing – review and editing; A. K.: conceptualization, funding acquisition, project administration, resources, supervision, methodology, writing – original draft, writing – review and editing.

Conflicts of interest

There are no conflicts to declare.

Acknowledgements

The authors acknowledge the National Science Foundation (DMR-EPM), NSF Graduate Research Fellowships Program (GRFP), and the University of Alabama Graduate Council Fellowship for financial support. The authors also wish to acknowledge the UA Analytical Research Center for instrumental and technical support.

References

1 S. Niu, N. Matsuhisa, L. Beker, J. Li, S. Wang, J. Wang, Y. Jiang, X. Yan, Y. Yun, W. Burnett, A. S. Y. Poon, J. B. H. Tok, X. Chen and Z. Bao, A wireless body area sensor network based on stretchable passive tags, *Nat. Electron.*, 2019, **2**(8), 361–368.

2 S.-K. Kang, J. Koo, Y. K. Lee and J. A. Rogers, Advanced Materials and Devices for Bioresorbable Electronics, *Acc. Chem. Res.*, 2018, **51**(5), 988–998.

3 W. Gao, S. Emaminejad, H. Y. Y. Nyein, S. Challa, K. Chen, A. Peck, H. M. Fahad, H. Ota, H. Shiraki, D. Kiriya, D.-H. Lien, G. A. Brooks, R. W. Davis and A. Javey, Fully integrated wearable sensor arrays for multiplexed in situ perspiration analysis, *Nature*, 2016, **529**(7587), 509–514.

4 G. Kettlgruber, M. Kaltenbrunner, C. M. Siket, R. Moser, I. M. Graz, R. Schwödiauer and S. Bauer, Intrinsically stretchable and rechargeable batteries for self-powered stretchable electronics, *J. Mater. Chem. A*, 2013, **1**(18), 5505–5508.

5 Y. Zhang, Y. Huang and J. A. Rogers, Mechanics of stretchable batteries and supercapacitors, *Curr. Opin. Solid State Mater. Sci.*, 2015, **19**(3), 190–199.

6 S. Huang, Y. Liu, Y. Zhao, Z. Ren and C. F. Guo, Flexible Electronics: Stretchable Electrodes and Their Future, *Adv. Funct. Mater.*, 2019, **29**(6), 1805924.

7 H. Stoyanov, M. Kollosche, S. Risse, R. Waché and G. Kofod, Soft Conductive Elastomer Materials for Stretchable Electronics and Voltage Controlled Artificial Muscles, *Adv. Mater.*, 2013, **25**(4), 578–583.

8 D. Qi, K. Zhang, G. Tian, B. Jiang and Y. Huang, Stretchable electronics based on PDMS substrates, *Adv. Mater.*, 2021, **33**(6), 2003155.

9 R. Morent, N. De Geyter, F. Axisa, N. De Smet, L. Gengembre, E. De Leersnyder, C. Leys, J. Vanfleteren, M. Rymarczyk-Machal and E. Schacht, Adhesion enhancement by a dielectric barrier discharge of PDMS used for flexible and stretchable electronics, *J. Phys. D: Appl. Phys.*, 2007, **40**(23), 7392.

10 A. Larmagnac, S. Eggenberger, H. Janossy and J. Vörös, Stretchable electronics based on Ag-PDMS composites, *Sci. Rep.*, 2014, **4**(1), 1–7.

11 T. K. Kim, J. K. Kim and O. C. Jeong, Measurement of nonlinear mechanical properties of PDMS elastomer, *Microelectron. Eng.*, 2011, **88**(8), 1982–1985.

12 J. Park, S. Wang, M. Li, C. Ahn, J. K. Hyun, D. S. Kim, D. K. Kim, J. A. Rogers, Y. Huang and S. Jeon, Three-dimensional nanonetworks for giant stretchability in dielectrics and conductors, *Nat. Commun.*, 2012, **3**(1), 916.

13 E. Berthier, E. W. Young and D. Beebe, Engineers are from PDMS-land, Biologists are from Polystyrenia, *Lab Chip*, 2012, **12**(7), 1224–1237.

14 S. Kuddannaya, J. Bao and Y. Zhang, Enhanced in vitro biocompatibility of chemically modified poly (dimethylsiloxane) surfaces for stable adhesion and long-term investigation of brain cerebral cortex cells, *ACS Appl. Mater. Interfaces*, 2015, **7**(45), 25529–25538.

15 I. Miranda, A. Souza, P. Sousa, J. Ribeiro, E. M. S. Castanheira, R. Lima and G. Minas, Properties and Applications of PDMS for Biomedical Engineering: A Review, *J. Funct. Biomater.*, 2021, **13**(1), 2.
16 S. H. Kim, J.-H. Moon, J. H. Kim, S. M. Jeong and S.-H. Lee, Flexible, stretchable and implantable PDMS encapsulated cable for implantable medical device, *Biomed. Eng. Lett.*, 2011, **1**, 199–203.
17 M. Dardouri, A. Bettencourt, V. Martin, F. A. Carvalho, C. Santos, N. Monge, N. C. Santos, M. H. Fernandes, P. S. Gomes and I. A. Ribeiro, Using plasma-mediated covalent functionalization of rhamnolipids on polydimethylsiloxane towards the antimicrobial improvement of catheter surfaces, *Biomater. Adv.*, 2022, **134**, 112563.
18 I. Johnston, M. Tracey, J. Davis and C. Tan, Micro throttle pump employing displacement amplification in an elastomeric substrate, *J. Micromech. Microeng.*, 2005, **15**(10), 1831.
19 M. Kim, B.-U. Moon and C. H. Hidrovo, Enhancement of the thermo-mechanical properties of PDMS molds for the hot embossing of PMMA microfluidic devices, *J. Micromech. Microeng.*, 2013, **23**(9), 095024.
20 Q. Wang, C. Du, J. Zhang, R. Lv and Y. Zhao, Sensitivity-enhanced temperature sensor based on PDMS-coated long period fiber grating, *Opt. Commun.*, 2016, **377**, 89–93.
21 G. Psarras, E. Manolakaki and G. Tsangaris, Dielectric dispersion and ac conductivity in—Iron particles loaded—polymer composites, *Composites, Part A*, 2003, **34**(12), 1187–1198.
22 Y. Shen, Z. Yue, M. Li and C. W. Nan, Enhanced Initial Permeability and Dielectric Constant in a Double-Percolating $Ni_{0.3}Zn_{0.7}Fe_{1.95}O_4$–Ni–Polymer Composite, *Adv. Funct. Mater.*, 2005, **15**(7), 1100–1103.
23 P. Barber, S. Balasubramanian, Y. Anguchamy, S. Gong, A. Wibowo, H. Gao, H. J. Ploehn and H.-C. Zur Loye, Polymer composite and nanocomposite dielectric materials for pulse power energy storage, *Materials*, 2009, **2**(4), 1697–1733.
24 R. Baptista, A. Mendão, F. Rodrigues, C. Figueiredo-Pina, M. Guedes and R. Marat-Mendes, Effect of high graphite filler contents on the mechanical and tribological failure behavior of epoxy matrix composites, *Theor. Appl. Fract. Mech.*, 2016, **85**, 113–124.
25 C. Pan, E. J. Markvicka, M. H. Malakooti, J. Yan, L. Hu, K. Matyjaszewski, C. Majidi and A. Liquid-Metal–Elastomer, Nanocomposite for Stretchable Dielectric Materials, *Adv. Mater.*, 2019, **31**(23), 1900663.
26 J. Zhang, R. Guo and J. Liu, Self-propelled liquid metal motors steered by a magnetic or electrical field for drug delivery, *J. Mater. Chem. B*, 2016, **4**(32), 5349–5357.
27 O. Oloye, J. F. Fernando, E. R. Waclawik, D. Golberg and A. P. O'Mullane, Galvanic replacement of liquid metal Galinstan with copper for the formation of photocatalytically active nanomaterials, *New J. Chem.*, 2020, **44**(35), 14979–14988.
28 S. Schreiber, M. Minute, G. Tornese, R. Giorgi, M. Duranti, L. Ronfani and E. Barbi, Galinstan thermometer is more accurate than digital for the measurement of body temperature in children, *Pediatric Emergency Care*, 2013, **29**(2), 197–199.
29 J. Y. Zhu, S.-Y. Tang, K. Khoshmanesh and K. Ghorbani, An integrated liquid cooling system based on galinstan liquid metal droplets, *ACS Appl. Mater. Interfaces*, 2016, **8**(3), 2173–2180.
30 D. Kim and J.-B. Lee, Magnetic-field-induced liquid metal droplet manipulation, *J. Korean Phys. Soc.*, 2015, **66**, 282–286.
31 M. D. Dickey, Stretchable and Soft Electronics using Liquid Metals, *Adv. Mater.*, 2017, **29**(27), 1606425.
32 T. Liu, P. Sen and C.-J. Kim, Characterization of nontoxic liquid-metal alloy galinstan for applications in microdevices, *J. Microelectromech. Syst.*, 2011, **21**(2), 443–450.
33 Y. Lin, J. Genzer and M. D. Dickey, Attributes, Fabrication, and Applications of Gallium-Based Liquid Metal Particles, *Adv. Sci.*, 2020, **7**(12), 2000192.
34 T. V. Neumann and M. D. Dickey, Liquid metal direct write and 3D printing: a review, *Adv. Mater. Technol.*, 2020, **5**(9), 2000070.
35 X. Wang and J. Liu, Recent advancements in liquid metal flexible printed electronics: Properties, technologies, and applications, *Micromachines*, 2016, **7**(12), 206.
36 C. Ladd, J. H. So, J. Muth and M. D. Dickey, 3D printing of free standing liquid metal microstructures, *Adv. Mater.*, 2013, **25**(36), 5081–5085.
37 M. D. Dickey, R. C. Chiechi, R. J. Larsen, E. A. Weiss, D. A. Weitz and G. M. Whitesides, Eutectic Gallium-Indium (EGaIn): A Liquid Metal Alloy for the Formation of Stable Structures in Microchannels at Room Temperature, *Adv. Funct. Mater.*, 2008, **18**(7), 1097–1104.
38 J.-H. So, J. Thelen, A. Qusba, G. J. Hayes, G. Lazzi and M. D. Dickey, Reversibly Deformable and Mechanically Tunable Fluidic Antennas, *Adv. Funct. Mater.*, 2009, **19**(22), 3632–3637.
39 Y. L. Park, B. R. Chen and R. J. Wood, Design and Fabrication of Soft Artificial Skin Using Embedded Microchannels and Liquid Conductors, *IEEE Sens. J.*, 2012, **12**(8), 2711–2718.
40 A. Koh, J. Sietins, G. Slipher and R. Mrozek, Deformable liquid metal polymer composites with tunable electronic and mechanical properties, *J. Mater. Res.*, 2018, **33**(17), 2443–2453.
41 X. Xue, D. Zhang, Y. Wu, R. Xing, H. Li, T. Yu, B. Bai, Y. Tao, M. D. Dickey and J. Yang, Segregated and Non-Settling Liquid Metal Elastomer via Jamming of Elastomeric Particles, *Adv. Funct. Mater.*, 2023, **33**(6), 2210553.
42 E. Bury and A. S. Koh, Multimodal Deformation of Liquid Metal Multimaterial Composites as Stretchable, Dielectric Materials for Capacitive Pressure Sensing, *ACS Appl. Mater. Interfaces*, 2022, **14**(11), 13678–13691.
43 E. A. Campo, 4 – Electrical Properties of Polymeric Materials, in *Selection of Polymeric Materials*, ed. E. A. Campo, William Andrew Publishing, Norwich, NY, 2008, pp. 141–173.

44 M. D. Bartlett, A. Fassler, N. Kazem, E. J. Markvicka, P. Mandal and C. Majidi, Stretchable, High-k Dielectric Elastomers through Liquid-Metal Inclusions, *Adv. Mater.*, 2016, **28**(19), 3726–3731.

45 C. Wang, C. Wang, Z. Huang and S. Xu, Materials and Structures toward Soft Electronics, *Adv. Mater.*, 2018, **30**(50), 1801368.

46 R. E. Calabrese, E. Bury, F. Haque, A. Koh and C. Park, Effects of filler composition, loading, and geometry on the dielectric loss, partial discharge, and dielectric strength of liquid metal polymer composites, *Composites, Part B*, 2022, **234**, 109686.

47 M. Rostaghi-Chalaki, K. Yousefpour, J. Klüss, M. Kurum, J. P. Donohoe and C. Park, Classification and comparison of AC and DC partial discharges by pulse waveform analysis, *Int. J. Electr. Power Energy Syst.*, 2021, **125**, 106518.

48 P. Wang, G. C. Montanari and A. Cavallini, Partial discharge phenomenology and induced aging behavior in rotating machines controlled by power electronics, *IEEE Trans. Ind. Electron.*, 2014, **61**(12), 7105–7112.

49 R. E. Calabrese, E. Bury, A. Koh and C. Park, In Effect of Particle Geometry on Electric Field Distribution, Partial Discharge, and Dielectric Strength of Iron–Polymer Composites, 2022 IEEE Electrical Insulation Conference (EIC), IEEE: 2022, pp. 90–93.

50 H. Zhu, S. Wang, M. Zhang, T. Li, G. Hu and D. Kong, Fully solution processed liquid metal features as highly conductive and ultrastretchable conductors, *npj Flexible Electron.*, 2021, **5**(1), 25.

51 O. Faruqe, F. Haque, P. C. Saha, I. Jovanovic, N. Uzelac and C. Park, Partial Incorporation of Nonlinear Resistive Field Grading Materials: A Strategy for Enhanced Field Reduction and Safety, *IEEE Trans. Dielectr. Electr. Insul.*, 2022, **30**(1), 474–483.

52 M. M. Tousi and M. Ghassemi, Characterization of nonlinear field-dependent conductivity layer coupled with protruding substrate to address high electric field issue within high-voltage high-density wide bandgap power modules, *IEEE J. Emerg. Sel. Top. Power Electron.*, 2019, **8**(1), 343–350.

53 A. Küchler, *High Voltage Engineering: Fundamentals-Technology-Applications*, Springer, 2017.

54 C. Chiew and M. H. Malakooti, A double inclusion model for liquid metal polymer composites, *Compos. Sci. Technol.*, 2021, **208**, 108752.

55 Y. Hu and C. Majidi, Dielectric Elastomers with Liquid Metal and Polydopamine-Coated Graphene Oxide Inclusions, *ACS Appl. Mater. Interfaces*, 2023, **15**(20), 24769–24776.

56 Y. Zang, F. Zhang, C.-A. Di and D. Zhu, Advances of flexible pressure sensors toward artificial intelligence and health care applications, *Mater. Horiz.*, 2015, **2**(2), 140–156.

57 S. R. A. Ruth, V. R. Feig, H. Tran and Z. Bao, Microengineering pressure sensor active layers for improved performance, *Adv. Funct. Mater.*, 2020, **30**(39), 2003491.

58 Z. Guo, L. Mo, Y. Ding, Q. Zhang, X. Meng, Z. Wu, Y. Chen, M. Cao, W. Wang and L. Li, Printed and flexible capacitive pressure sensor with carbon nanotubes based composite dielectric layer, *Micromachines*, 2019, **10**(11), 715.

59 Z. Ma, K. Zhang, S. Yang, Y. Zhang, X. Chen, Q. Fu and H. Deng, High-performance capacitive pressure sensors Fabricated by introducing dielectric filler and conductive filler into a porous dielectric layer through a Biomimic strategy, *Compos. Sci. Technol.*, 2022, **227**, 109595.

60 S. M. A. Jiménez and R. M. McMeeking, A constitutive law for dielectric elastomers subject to high levels of stretch during combined electrostatic and mechanical loading: Elastomer stiffening and deformation dependent dielectric permittivity, *Int. J. Non Linear Mech.*, 2016, **87**, 125–136.

61 L. Di Lillo, A. Schmidt, D. A. Carnelli, P. Ermanni, G. Kovacs, E. Mazza and A. Bergamini, Measurement of insulating and dielectric properties of acrylic elastomer membranes at high electric fields, *J. Appl. Phys.*, 2012, **111**(2), 024904.